Scripta Materialia 116 (2016) 76–81

Contents lists available at ScienceDirect

Scripta Materialia

journal homepage: www.elsevier.com/locate/scriptamat

Regular Article

Non-aqueous nanoporous gold based supercapacitors with high specific energy

Ying Hou [a,b], Luyang Chen [b], Akihiko Hirata [b], Takeshi Fujita [b], Mingwei Chen [a,b,c,*]

[a] Key Laboratory of Interface Science and Engineering in Advanced Materials, Taiyuan University of Technology, Ministry of Education, Taiyuan 030024, PR China
[b] World Premier International (WPI) Research Center, Advanced Institute for Materials Research, Tohoku University, Sendai 980-8577, Japan
[c] CREST, Japan Science and Technology Agency (JST), Saitama, 332-0012, Japan

ARTICLE INFO

Article history:
Received 20 November 2015
Received in revised form 8 January 2016
Accepted 10 January 2016
Available online 7 February 2016

Keywords:
Nanoporous gold
Polypyrrole
Supercapacitor
Ionic liquid
Dealloying

ABSTRACT

In this study, we report that the supercapacitor performance of polypyrrole (PPy) in non-aqueous electrolytes can be dramatically improved by highly conductive nanoporous gold which acts as both the support of active PPy and the current collector of supercapacitors. The excellent electronic conductivity, rich porous structure and large surface area of the nanoporous electrodes give rise to a high specific capacitance and low internal resistance in non-aqueous electrolytes. Combining with a wide working potential window of ~2 V, the non-aqueous PPy-based supercapacitors show an extraordinary energy density and power density.

1. Introduction

The electrochemical energy storage devices play a critical role in green energy innovation for energy harvesting and power delivery [1–4]. Among various electrochemical energy storage devices, electrochemical supercapacitors have drawn increasing attention for environment-friendly applications, such as portable electronics, hybrid electric vehicles and memory backup systems because of their high power density, rapid charge/discharge rate and high specific capacitance [5–7]. On the basis of the mechanisms of charge storage, the electrochemical supercapacitors can be divided into two types. One is the electrochemical double layer capacitors (EDLC) which store energy by non-Faradic surface ion adsorption [8,9]. The other is the pseudocapacitors which realize high energy storage through fast Faradic redox reactions and intercalation of ions at interfaces between active electrode materials, such as conducting polymers [10,11] and transition metal oxides [12,13], and electrolytes. Although the pseudocapacitors have a relatively high capacitance compared to EDLC, the energy density of pseudocapacitors is still much lower than that of Li-ion batteries, which is limited by their narrow working potentials in aqueous solutions and/or insufficient utilization of pseudocapacitive reactions in non-aqueous electrolytes.

The energy density (E) of a supercapacitor is determined by the equation: $E = 0.5C_sV^2$, where C_s is the specific capacitance of the supercapacitor and V is the working potential of the cell [14]. Usually, supercapacoitors have a narrow potential window, which is lower than 1.2 V in aqueous solutions due to the restriction of thermodynamic potential of water electrolysis. Hence, a non-aqueous solution with large stable working potential is expected to enlarge the energy storage capacity of pseudocapacitors [15,16]. Recently, room temperature ionic liquids (RTILs) have been investigated as non-aqueous solutions for a high working potential of supercapacitors, which are promising electrolytes owing to their high electrochemical and thermal stability, wide liquid-phase range, low vapor pressure and non-flammability.

Among many pseudocapacitive materials, polypyrrole (PPy) has attracted considerable attentions as a promising electrode material own to its low material costs, high theoretical capacitance, environmental friendliness and easy synthesis [17,18]. Similar to other pseudocapactive materials, the energy densities of PPy-based capacitors are largely limited by a narrow working potential window in aqueous solutions. Since conducting polymers usually have a lower electric conductivity and lower specific capacitance than transition metal oxides in non-aqueous solutions, there are very few attempts on non-aqueous PPy-based supercapacitors [14,19,20]. Although these non-aqueous supercapacitors have an enlarged operation voltage window, the improvement in the energy density of the PPy-based supercapacitors is minimal because of high internal resistance and decreased specific capacitance. Therefore, enhancing the electric conductivity and specific capacitance of PPy-based electrodes in non-aqueous electrolytes is essential to realize the high energy density.

Dealloyed nanoporous metals with a high electrical conductivity, large specific surface area and excellent affinity with active materials have recently been utilized as both supports of pseudocapacitive

* Corresponding author at: WPI-AIMR, Tohoku University, Sendai 980-8577, Japan.
E-mail address: mwchen@wpi-aimr.tohoku.ac.jp (M. Chen).

http://dx.doi.org/10.1016/j.scriptamat.2016.01.016
1359-6462/

materials and current collectors of supercapacitors and actuators [8,13,21–24]. The metal based three-dimensional electrodes can obviously enhance the specific capacitance of poor-conductive active materials and effectively reduce the device weight and volume, simultaneously. In the context of our previous work in preparing high-conductive PPy-nanoporous gold (NPG) hybrid composites with a high specific capacitance [25,26], in this study we developed PPy-NPG based non-aqueous supercapacitors with a wide operation voltage window and high energy density by using RTIL as electrolytes.

2. Experimental section

2.1. Synthesis of NPG and PPy-NPG hybrid composites

All the chemicals were of analytical grade and used without further purification. Nanoporous gold (NPG) films with a thickness of about 100 nm were fabricated by free chemical corrosion using commercial $Au_{35}Ag_{65}$ (at. %) alloy leaves in a concentrated HNO_3 solution (wt. 69%) for 6 h at room temperature. Deionized water (18.2 MΩ·cm) was utilized to rinse as-prepared NPG for three times in order to remove the residual chemical substances within pore channels after the nanoporous structure of NPG was taken away from the acid solution. The as-prepared NPG films were then fixed to polyethylene terephthalate (PET) plates by annealing NPG/PET at the temperature of 80 °C for convenient handling as flexible electrodes

PPy-NPG composites were prepared by an electrochemical plating method [25,27]. 1.382 mL Pyrrole (99.0% Wako Pure Chemical Industries) and 1.6 mL $HClO_4$ (Kanto Chemical Co., Inc.) were dissolved in 200 mL distilled water to form a 0.1 M Pyrrole/$HClO_4$ solution. The NPG/PET plates were immersed into the electrolyte at room temperature. The electroplating was performed in a standard three-electrode system with a platinum sheet as the counter electrode, Ag/AgCl as the reference electrode, and an NPG/PET plate as the working electrode. The anodic oxidation synthesis of pyrrole on NPG was conducted by a cyclic voltammetry (CV) method with a potential window ranging from −0.2 V to 0.9 V. The loading amount of PPy was controlled by the cycling number of plating. The mass of deposited PPy was determined based on the equation: $m = QM/zF = QM_M/(2 + y)F$, where m is the mass of the deposited PPy, Q is polymerizing charge, y is a stoichiometric factor evaluating the PPy insertion degree (=0.2, based on Ref. [28]), and F is the faradic constant [29]. M_M is the molecular weight of the polymer monomer unit ($M_M = M_{Py} - 2$), and M_{Py} is pyrrole molecular weight.

2.2. Microstructure characterization

The microstructure of the as-synthesized PPy-NPG composites was characterized by a JEOL JIB-4600F scanning electron microscope (SEM) and a JEOL JEM-2100F transmission electron microscope (TEM) equipped with double spherical aberration correctors.

2.3. Assembly of PPy-NPG supercapacitors and electrochemical measurements

Two-electrode supercapacitor devices were constructed with two PPy-NPG/PET plates as the electrodes separated by a thin cotton paper (~40 μm in thickness, BemlieseTM). The electrochemical properties and capacitive performances of the PPy-NPG supercapacitors were investigated using a standard two-electrode electrochemical system. The CV and charge/discharge curves were measured at different scan rates and current densities using an electrochemical station (Ivium Technology). Three kinds of RTIL were chosen as electrolytes in this study, including 1-Ethyl-3-methylimidazolium bis(fluorosulfonyl)imide (EMI-FSI), 1-Ethyl-3-methylimidazolium Dicyanamide (EMI-DCA) and N,N-diethyl-N-methyl-N-(2-methoxyethyl)ammonium bis(trifluoromethanesulfonyl)imide (DEME-TFSI).

3. Results and discussion

Fig. 1(a) exhibits the top view SEM image of 1-cycle plated PPy-modified NPG with an open nanoporous structure. The average size of pore channels and gold ligaments of as-prepared NPG were measured to be ~40 nm using a rotational fast Fourier transform method [30]. The thickness of the NPG current collector is about 100 nm. The ultra-thin current collector provides excellent rate performance by eliminating the slow diffusion of the RTIL electrolytes in nano-sized pore channels. The bright-field TEM image shows that the PPy coating forms a core-shell structure in which the conducting polymer layer displays bright contrast as the shell that uniformly covers the internal surface of the dark-contrast metal ligaments (Fig. 1(b)). The core-shell structure with open porosity promises the good conductivity of the PPy-NPG composite and the effective rapid ion transport of electrolytes within the porous electrodes. A high-resolution TEM (HRTEM) image (Fig. 1(c)) reveals the well-bonded PPy/Au interface and the deposited PPy has an amorphous structure without any well-defined periodic lattice. By tuning the cycle number of the electrochemical plating, the loading amount and the layer thickness of PPy can be well controlled. The loading amount of PPy gradually increases with the cycling number from 1 to 5. As shown in Fig. S1(a–e), the samples plated for 1 to 3-cycles exhibit open structure which is similar to pure NPG due to the weak contrast of PPy in the SEM images. When the cycle number increases to 4 and 5, some nanopores are blocked by the excess PPy which grows on the external surface of the NPG films. Quantitative measurements indicate the nearly linear dependence of the loaded PPy amount with the plating cycle (Fig. S1(f)).

The PPy-NPG composites were assembled into a two-electrode supercapacitor for electrochemical measurements. Two PPy-NPG films were used as working electrode and counter electrode, respectively. A piece of cotton paper was utilized as separator between two PPy-NPG electrodes for preventing short circuit and free mobility of cations and anions from non-aqueous electrolytes. Since the capacitive Performance of the PPy-NPG supercapacitors shows the strong dependence on the loading amount of PPy, the capacitance performance of the electroplated NPG with different PPy loading amounts was first investigated to optimize the loading amount of PPy. Fig. S2(a–c) reveal the CV curves

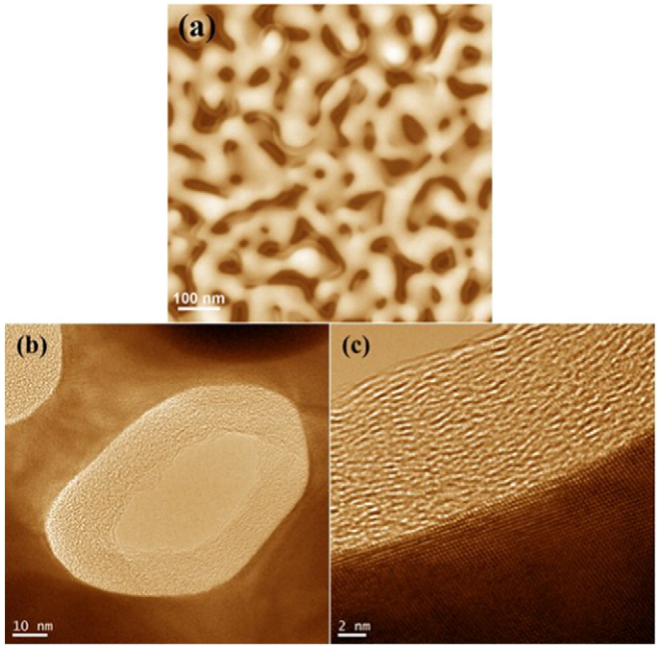

Fig. 1. (a) Representative SEM and (b) TEM images of the PPy-NPG composite with electroplated PPy. (c) HRTEM image showing the interfacial structures of the PPy-NPG composite.

of the PPy-NPG supercapacitors with PPy plating cycles from 1 to 5 in the three ionic liquids at the scan rate of 10 mV/s. The specific capacitance of PPy-NPG supercapacitor gradually decreased from 1-cycle to 5-cycle as shown in Fig. S2(d). The decrease of the specific capacitance with the loading amount of PPy may be attributed to that the excess PPy blocks the nanopores and prevents the free access of ions through the nanopore channels of NPG.

Fig. 2(a–c) show the CV curves of the optimized PPy-NPG supercapacitors obtained at different scan rates in three ionic liquids, DEME-TFSI, EMI-DCA and EMI-FSI. The stable working potentials were determined to be 1.8 V, 1.5 V, and 2.0 V in DEME-TFSI, EMI-DCA and EMI-FSI, respectively. When the applied potentials are above those values, irreversible reactions occur and lead to the decomposition of PPy and/or RTIL. The CV curves present a good symmetric shape during forward and backward scans both at the low scan rate of 10 mV/s and high scan rates of 1000 mV/s, suggesting the good capacitive ability of the PPy-NPG supercapacitors with the RTIL electrolytes. The area of the CV curve indicates the capacitive ability of the active material and a larger area proves a higher specific capacitance at the same scan rate. As shown in Fig. 2(a) to (c), the CV areas of the three RTIL electrolytes are evidently different and increase from DEME-TFSI to EMI-DCA and EMI-FSI. The specific capacitance and specific capacity of the PPy-NPG supercapacitors at different scan rates in three ionic liquids were calculated on the basis of the CV curves (Fig. 2(d)). The total mass of active materials on the two electrodes of the supercapacitors was used to calculate the specific capacitances. The specific capacitance is strongly dependent on the ionic liquid electrolytes. The PPy-NPG supercapacitor in the EMI-FSI electrolyte achieves the highest specific capacitance in comparison with other two ionic liquid electrolytes. As the scan rate increases from 10 to 1000 mV/s, the specific capacitance of the PPy-NPG supercapacitor gradually reduces. However, the specific capacitance of PPy-NPG supercapacitors can still retain a high value even at fast scan rate of 1000 mV/s, which indicates the stable capacitive performance of PPy-NPG in the three ionic liquid electrolytes.

Representative galvanostatic charge/discharge curves of the PPy-NPG supercapacitors as the function of the current densities in three ionic liquid electrolytes are illustrated in Fig. 3(a–c). The working potentials of PPy-NPG supercapacitors in DEME-TFSI, EMI-DCA and EMI-FSI electrolytes are 1.8 V, 1.5 V, and 2 V, respectively, which are consistent with the working potentials determined by CV tests (Fig. 2). The discharge time of the supercapacitor decreases with the increase of current density. At the same current density, longer discharge time promises higher specific capacitance. The difference of charge/discharge time at the same current density in various electrolytes indicates that the capacitive performance of the PPy-NPG supercapacitors strongly depend on the electrolytes. The specific capacitance of the symmetric supercapacitors at different current densities is calculated according to the charge/discharge curves by the formula $C_s = i/[-(\Delta E/\Delta t)m]$, where i is the applied current; $-\Delta E/\Delta t$, the slope of the discharge curve after the voltage drop at the beginning of each discharge (ΔE_{IR}); and m stands for the mass of the total active material of two electrodes [31]. Moreover, the specific capacity is calculated by the formula: $C_s = i*\Delta t/m$, where i is the applied current;Δt is the discharge time; and m stands for the mass of the total active material of two electrodes. Fig. 3(d) elucidates the specific capacitance of the non-aqueous PPy-NPG supercapacitors as the function of current density in three ionic liquid electrolytes. The results are consistent with the CV measurements that the specific capacitance of PPy-NPG shows the highest values in EMI-FSI at different current densities compared with other two ionic liquids. At the discharge current density of 2 A/g, the specific capacitance of the PPy-NPG supercapacitor reaches ~112 F/g (~62 mAh/g) in EMI-FSI. Even at the high current density of 20 A/g, the specific capacitance is still as high as ~100 F/g, comparable to that of aqueous PPy-based supercapacitors.

The plots in Fig. 4(a–c) show the coulombic efficiencies (η) of the non-aqueous supercapacitors with different ionic liquid electrolytes. Based on the charge/discharge curves, η is determined by the ratio of discharge time (t_d) and charge time (t_c), $\eta = t_d/t_c \times 100\%$ [32]. The PPy-NPG supercapacitor in EMI-FSI can attain a high coulombic

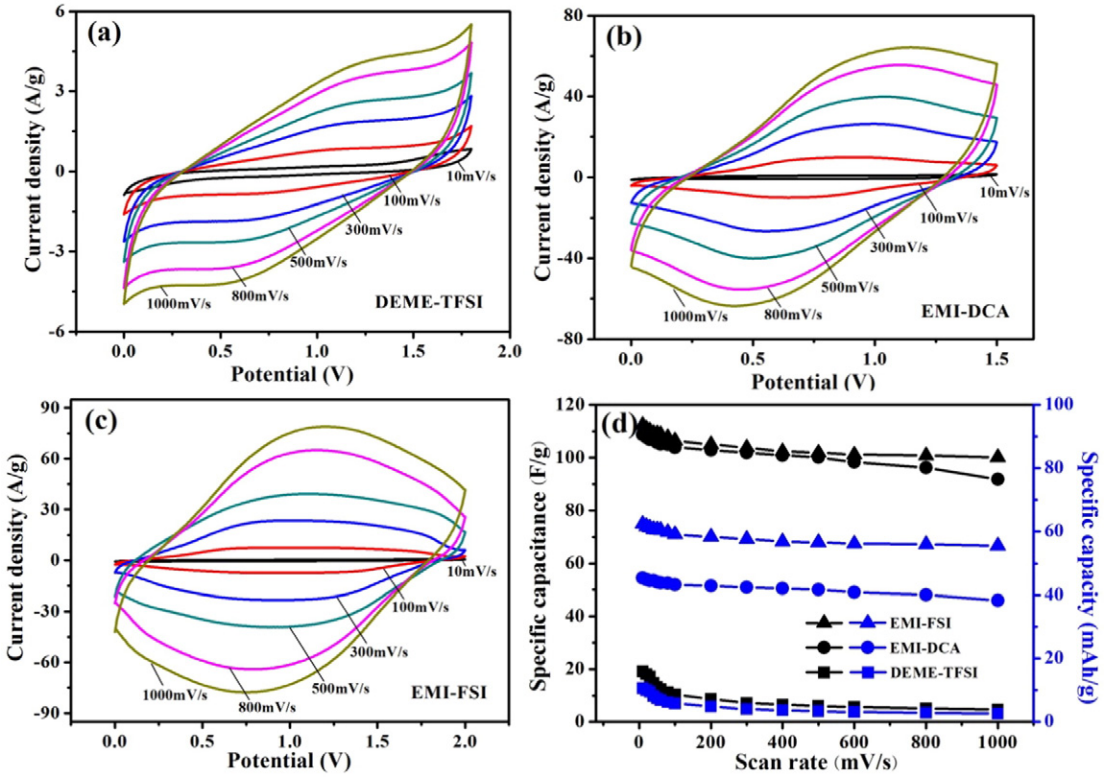

Fig. 2. CV curves of PPy-NPG supercapacitors at different scan rates in the ionic liquids of (a) DEME-TFSI, (b) EMI-DCA, and (c) EMI-FSI. (d) Specific capacitance and specific capacity of the PPy-NPG supercapacitors at different scan rates in three ionic liquids.

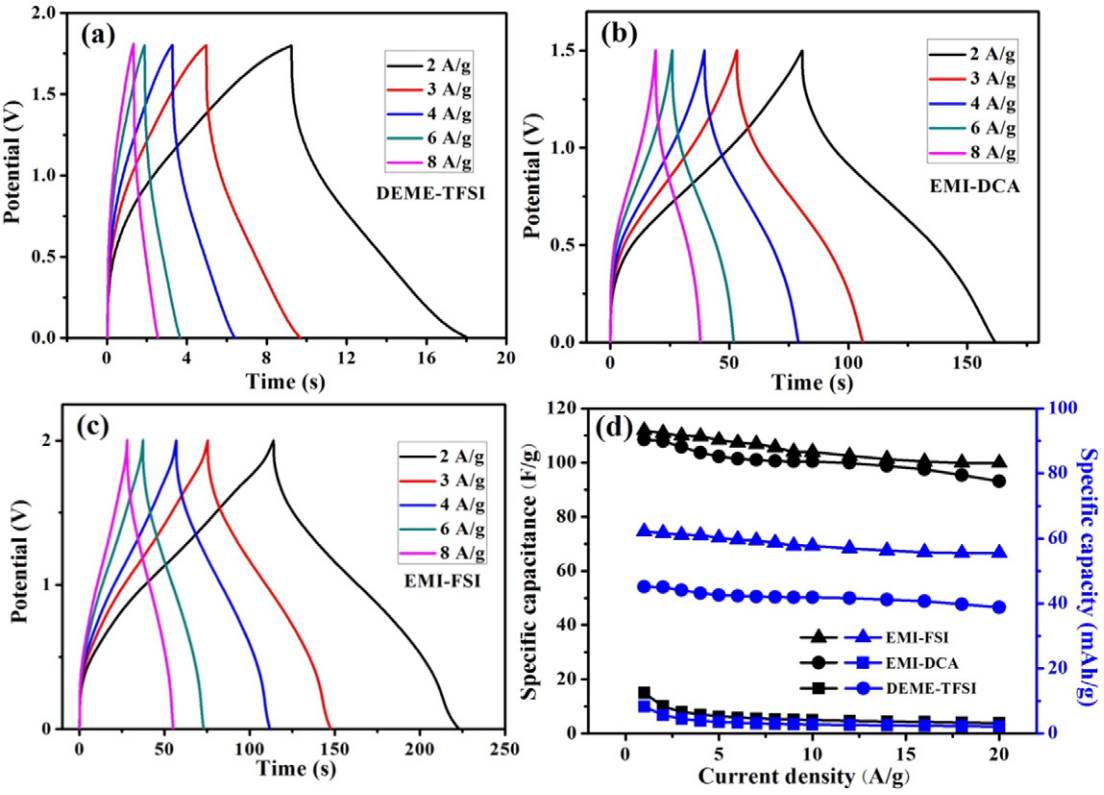

Fig. 3. Galvanostatic charge/discharge curves of PPy-NPG supercapacitors at different current densities in the ionic liquids of (a) DEME-TFSI, (b) EMI-DCA, and (c) EMI-FSI. (d) Specific capacitance and specific capacity of PPy-NPG supercapacitors obtained at different current densities in three ionic liquids.

efficiency, better than 96%, at different current densities, indicating fully reversible redox reactions during charge and discharge. The internal resistance (R) of the supercapacitor cells is determined by the initial voltage drop (ΔV_{IR}) and discharge current density, i.e., $R = \Delta V_{IR}/I$ [33]. Fig. 4(d–f) exhibit the internal resistance of the PPy-NPG supercapacitors in three ionic liquids at different current densities. The internal resistance gradually reduces with current density increases. From discharge curves (Fig. 3), the obvious voltage drops prove that the supercapacitors have large equivalent series resistance (ESR). The measured ESR originates from all cell components, including current collectors, electrodes, electrolyte and separator, and therefore only a portion of the measured resistance can be attributed to the electrode material itself. Since ionic liquids have lower mobility and conductivity compared with aqueous electrolytes, the voltage drops are evidently higher than those in aqueous electrolytes. Because of the electrode materials are essentially the same in the three non-aqueous supercapacitors, the observed difference in the internal resistance is mainly influenced by the transport properties of the electrolytes, which include the ionic conductivity, mobility, volume, steric hindrance, solvent fluidity, and so on. The strong charge transfer between EMI-FSI and PPy leads to the highest specific capacitance and lowest internal resistance of the PPy-NPG supercapacitor in EMI-FSI (Fig. 4(d–f)). The internal resistance of the PPy-NPG supercapacitor with EMI-FSI is ~200 Ω, while those of the PPy-NPG supercapacitors using EMI-DCA and DEME-TFSI as electrolytes are ~300 Ω and ~1600 Ω, respectively. Moreover, the internal resistance of the PPy-NPG supercapacitor only has minor changes at the different current densities in EMI-FSI, demonstrating the stable performance of the PPy-NPG supercapacitor with the EMI-FSI electrolyte.

In order to further investigate the capacitive performance of PPy-NPG supercapacitors in the ionic liquids. The electrochemical impedance (EIS) measurements of the devices were performed from 100 kHz to 0.1 Hz with the alternative current amplitude of 50 mV. The Nyquist plots are shown in Fig. S3(a). In the high frequency region, the semicircle corresponds to the charge-transfer resistance (R_{ct}) at the electrode/electrolyte interface or intrinsic charge-transfer resistance of the porous electrode [34]. The lowest radius shown in the inset of Fig. S3(a) indicates that the PPy-NPG has the highest efficiency of charge transport in EMI-FSI. The intercept on X axis (R_s) means the bulk electrolyte solution resistance, the intrinsic resistance of active material and the electron transfer resistance at the current collector/electrode boundary. The PPy-NPG electrode in EMI-FSI still exhibits the lowest R_s value than in other ionic liquids. The smaller resistances of R_{ct} and R_s both result from strong charge transfer between EMI-FSI and PPy as well as the intrinsically high conductivity and low viscosity of EMI-FSI, which increase the electric conductivity and further enhance the charge storage capability.

Although the specific capacitance of the PPy-NPG electrodes in RTIL is not as high as that in aqueous electrolytes, the wide potential windows give rise to the higher energy density and power density of the non-aqueous PPy-NPG supercapacitors. The specific power density P and energy density E were calculated using the equations: $P = V^2/(4Rm)$ and $E = 0.5CV^2$, respectively [5]. Here, V is the cutoff voltage, C is the measured device capacitance, and R is the internal resistance of the devices. The specific Ragone plot of energy density and power density of the PPy-NPG supercapacitors in non-aqueous electrolytes is shown in Fig. S3(b). The PPy-NPG supercapacitor in the EMI-FSI electrolyte has the energy density of ~60 Wh/kg and the power density of ~40 kW/kg, which are obviously higher than those of EMI-DCA and DEME-TFSI.

Due to the poor electronic and ionic conductivities which limit the rapid faradaic reduction and oxidation reactions with the non-aqueous ions, PPy usually has low specific capacitance in ionic liquid electrolytes. NPG as both support and current collector can dramatically improve the conductivity of PPy in ionic liquids. The excellent conductivity of NPG [35] and chemically well-bonded Au/PPy interface give rise to high conductivity of PPy and the low internal resistance as well as high coulombic efficiency for realization of the high capacitance of PPy. Therefore, the outstanding capacitive performance of PPy in the EMI-FSI RTIL underlines the importance of electric conductivity in the

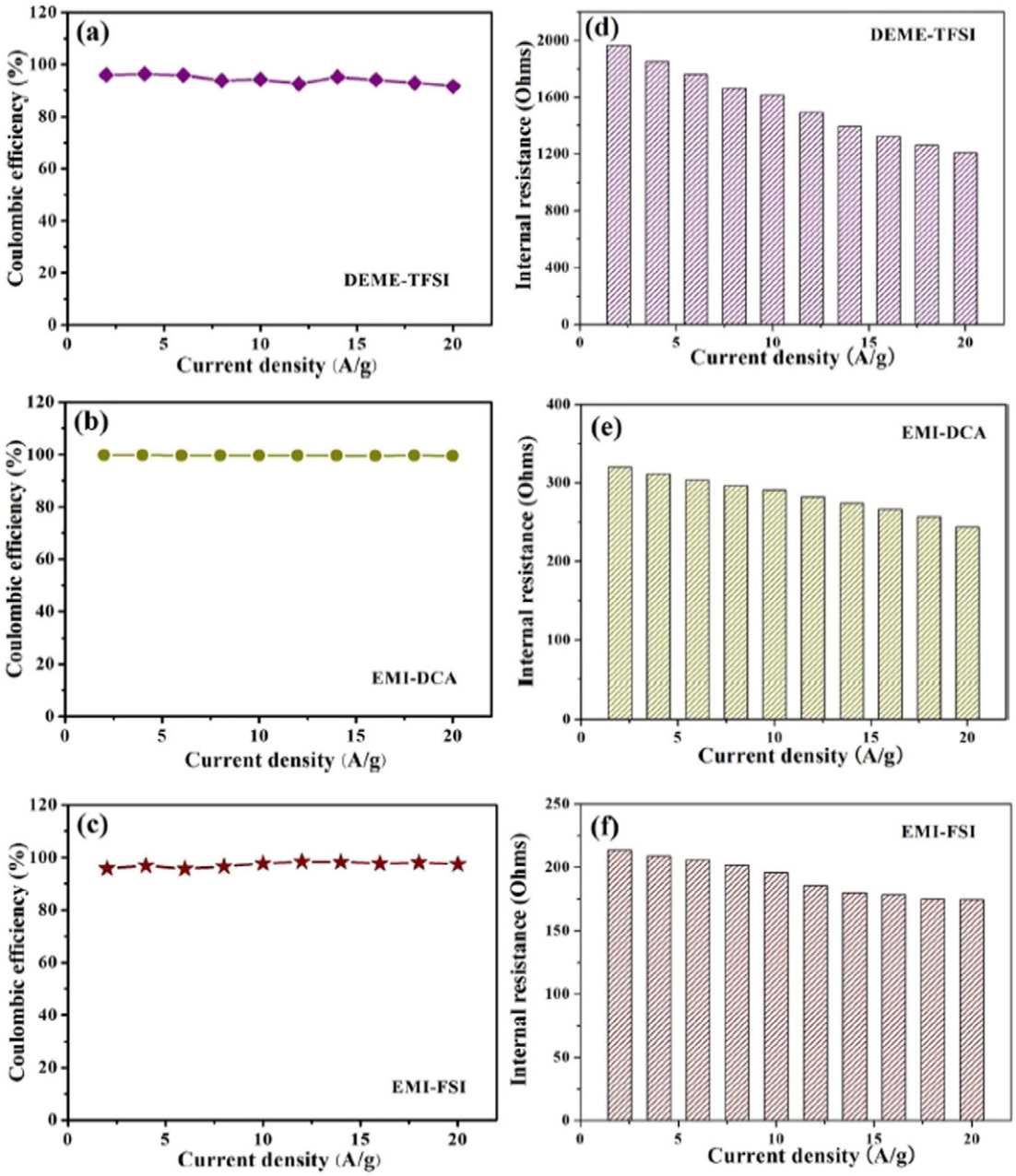

Fig. 4. (a–c) Coulombic efficiency and (d–f) internal resistance obtained at different current densities of the PPy-NPG supercapacitors in three ionic liquids.

electrode reactions between organic pseudocapacitive materials and non-aqueous electrolytes in implementation of high capacitance at a high operation voltage for high energy storage.

4. Conclusion

In summary, we successfully developed non-aqueous PPy-NPG based supercapacitors with wide potential windows and high energy densities by using ionic liquids as electrolytes. The enhanced conductivity of PPy by highly conductive NPG leads to the realization of a high specific capacitance and low internal resistance of PPy-based electrodes in ionic liquids at a high operation voltage. The large capacitance of ~112 F/g together with a high working potential of 2.0 V can be achieved in the EMI-FSI RTIL. Therefore, the non-aqueous PPy-NPG supercapacitor possesses the high energy density of ~60 Wh/kg and the power density of ~40 kW/kg, offering the practical energy density of ~15–20 Wh/kg after considering the conversion factor of 0.26 to 0.32.

Author Contributions

The manuscript was written through contributions of all authors. All authors have given approval to the final version of the manuscript.

Notes

The authors declare no competing financial interest.

Acknowledgments

This research was sponsored by “Interface Science for Highly Efficient Energy Utilization”, CREST, JST; and the State Key Laboratory for Advanced Metals and Materials, University of Science and Technology Beijing.

Appendix A. Supplementary data

Supplementary data to this article can be found online at http://dx.doi.org/10.1016/j.scriptamat.2016.01.016.

References

[1] M. Winter, R.J. Brodd, Chem. Rev. 104 (2004) 4245.
[2] L.L. Zhang, X.S. Zhao, Chem. Soc. Rev. 38 (2009) 2520.
[3] R. Liu, S.B. Lee, J. Am. Chem. Soc. 130 (2008) 2942.
[4] A.S. Arico, P. Bruce, B. Scrosati, J.M. Tarascon, W. Van Schalkwijk, Nat. Mater. 4 (2005) 366.
[5] P. Simon, Y. Gogotsi, Nat. Mater. 7 (2008) 845.
[6] K.H. An, W.S. Kim, Y.S. Park, Y.C. Choi, S.M. Lee, D.C. Chung, D.J. Bae, S.C. Lim, Y.H. Lee, Adv. Mater. 13 (2001) 497.
[7] J.R. Miller, P. Simon, Science 321 (2008) 651.
[8] X.Y. Lang, H.T. Yuan, Y. Iwasa, M.W. Chen, Scr. Mater. 64 (2011) 923.
[9] J.S. Huang, B.G. Sumpter, V. Meunier, Angew. Chem. Int. Ed. 47 (2008) 520.
[10] L. Nyholm, G. Nyström, A. Mihranyan, M. Strømme, Adv. Mater. 23 (2011) 3751.
[11] T.B. Schon, P.M. DiCarmine, D.S. Seferos, Adv. Energy Mater. 4 (2014) 1301509.
[12] T. Brezesinski, J. Wang, S.H. Tolbert, B. Dunn, Nat. Mater. 9 (2010) 146.
[13] L.Y. Chen, Y. Hou, J.L. Kang, A. Hirata, T. Fujita, M.W. Chen, Adv. Energy Mater. 3 (2013) 851.
[14] J.-K. Chang, M.-T. Lee, C.-W. Cheng, W.-T. Tsai, M.-J. Deng, Y.-C. Hsieh, I.W. Sun, J. Mater. Chem. 19 (2009) 3732.
[15] M. Armand, F. Endres, D.R. MacFarlane, H. Ohno, B. Scrosati, Nat. Mater. 8 (2009) 621.
[16] J.F. Wishart, Energy Environ. Sci. 2 (2009) 956.
[17] P.G. Bruce, B. Scrosati, J.-M. Tarascon, Angew. Chem. Int. Ed. 47 (2008) 2930.
[18] G.A. Snook, P. Kao, A.S. Best, J. Power Sources 196 (2011) 1.
[19] M.-J. Deng, J.-K. Chang, C.-C. Wang, K.-W. Chen, C.-M. Lin, M.-T. Tang, J.-M. Chen, K.-T. Lu, Energy Environ. Sci. 4 (2011) 3942.
[20] T.M. Benedetti, F.F.C. Bazito, E.A. Ponzio, R.M. Torresi, Langmuir 24 (2008) 3602.
[21] X.Y. Lang, A. Hirata, T. Fujita, M.W. Chen, Nat. Nanotechnol. 6 (2011) 232.
[22] E. Detsi, S. Tolbert, S. Punzhin, J.M. De Hosson, J. Mater. Sci. 51 (2016) 615.
[23] E. Detsi, S. Punzhin, J. Rao, P.R. Onck, J.T.M. De Hosson, ACS Nano 6 (2012) 3734.
[24] E. Detsi, P. Onck, J.T.M. De Hosson, ACS Nano 7 (2013) 4299.
[25] Y. Hou, L.Y. Chen, L. Zhang, J.L. Kang, T. Fujita, J.H. Jiang, M.W. Chen, J. Power Sources 225 (2013) 304.
[26] Y. Hou, L. Zhang, L.Y. Chen, P. Liu, A. Hirata, M.W. Chen, Phys. Chem. Chem. Phys. 16 (2014) 3523.
[27] F.H. Meng, Y. Ding, Adv. Mater. 23 (2011) 4098.
[28] S. Park, S. Jayaraman, MRS Bull. 28 (2003) 585.
[29] E.M. Genies, G. Bidan, J. Electroanal. Chem. 149 (1983) 101.
[30] T. Fujita, M.W. Chen, Jpn. J. Appl. Phys. 47 (2008) 1161.
[31] L.B. Hu, J.W. Choi, Y. Yang, S.M. Jeong, F. La Mantia, L.-F. Cui, Y. Cui, Proc. Natl. Acad. Sci. 106 (2009) 21490.
[32] X.Y. Lang, L. Zhang, T. Fujita, Y. Ding, M.W. Chen, J. Power Sources 197 (2012) 325.
[33] M. Kaempgen, C.K. Chan, J. Ma, Y. Cui, G. Gruner, Nano Lett. 9 (2009) 1872.
[34] J.L. Kang, L.Y. Chen, Y. Hou, C. Li, T. Fujita, X.Y. Lang, A. Hirata, M.W. Chen, Adv. Energy Mater. 3 (2013) 857.
[35] T. Fujita, H. Okada, K. Koyama, K. Watanabe, S. Maekawa, M.W. Chen, Phys. Rev. Lett. 101 (2008) 166601.